Appl. Phys. B 66, 213–216 (1998)

Applied Physics B
Lasers
and Optics

High-harmonic generation of mid-IR pulses in simple liquids

R. Zürl, H. Graener

Fachbereich Physik, Martin-Luther-Universität Halle-Wittenberg, 06099 Halle, Germany

Received: 2 April 1997/Revised version: 18 June 1997

Abstract. The generation of the third, fifth and seventh harmonic of picosecond mid-IR pulses in a simple liquid with reasonable efficiencies is reported and discussed. The observed intensity dependence for the jth harmonic was I^j as expected. The analysis of the frequency dependence indicates the strong influence of vibrational resonances, which were found here for the first time. Near the fundamental resonance the jth harmonic generation has to be described as a $(j+3)$ wave mixing experiment due to the necessary inclusion of the population of the corresponding vibrational state.

PACS: 33.70; 42.65

For rare gases, high-harmonic generation has been known since 1978 [1], and has since been used to generate radiation with wavelengths of 7.4 nm by 143rd harmonic generation [2]. All the processes were enhanced by electronic resonances. The state of high harmonic generation to be discussed in this paper is close that of [1] and was detected during studies of vibrational population relaxation processes in liquid chloroform. Those experiments require a strong infrared pulse (resonantly tuned to a molecular transition) to achieve several percent of population, which is subsequently monitored either by IR transmission changes [3–7] or spontaneous anti-Stokes Raman scattering [8–11]. The formal analysis of these experiments shows that the first is a third-order experiment described by $\chi^{(3)}(-\omega'; \omega, -\omega, \omega')$ with ω as pump and ω' as probe frequency, whereas the latter is a fifth-order experiment given by $\chi^{(5)}(-\omega_R; \omega, -\omega, \omega_{PR}, -\omega_{PR}, \omega'_R)$ with ω_{PR} as probe frequency and ω_R as scattered Raman frequency. Using pulse durations of several picoseconds [5, 10], energy densities of the order of $0.1\,\mathrm{J\,cm^{-2}}$ (corresponding to intensities of $10\,\mathrm{GW\,cm^{-2}}$) are needed to achieve a detectable population. Under these excitation conditions, other high-order nonlinear processes may occur. In the following, high-harmonic generation (third to seventh order) is reported and discussed.

1 Experimental results

The experimental setup was originally designed to study vibrational population relaxation processes after a strong resonant IR excitation with the help of spontaneous anti-Stokes Raman scattering [10, 11]. Tunable IR pulses (pulse duration ≈ 4 ps, tuning range 2500–4000 $\mathrm{cm^{-1}}$, typical pulse energy 20–40 μJ were derived from an APM–FCM Nd:YLF Laser (repetition rate 60 Hz), which pumps a multi-step optical parametric frequency conversion setup. For the Raman probing, a minor part of the Nd:YLF single pulse is frequency doubled.

The probe setup is shown in Fig. 1a. The focused pulses (beam diameters approx. 100 μm) are overlapped in the sample (length 100 μm). The scattered light is collected and collimated by a $f/1.4$ objective lens, it passes a Notch filter, and is focused into the entrance slit (width 100 μm) of a $f = 64$ cm spectrometer with a 150 lines/mm grating. The scattered light is monitored with an LN-cooled, back-illuminated CCD camera (1100×300 pixels).

All experiments described in the following are performed on liquid chloroform in an Infrasil quartz cell. For an IR frequency of $3020\,\mathrm{cm^{-1}}$ (the absorption frequency of a CH-stretching vibration) the observed intensity distribution on the CCD chip (with five seconds integration time and spectrometer center wavelength of approx. 550 nm) is shown in Fig. 1b. Besides the strong vertical line (corresponding to the Rayleigh scattering of the green light) and the stripes that are due to the spontaneous Raman scattering (of the green pulses), an additional intensity with a different spatial shape at wavelengths above 600 nm is observed. Blocking the green pulses only, we found that this additional intensity remained. Changing the IR frequency, we established that the intensity shifts according to $\nu = 5\nu_{IR}$. From these findings, we concluded that this additional peak is due to fifth-harmonic generation in the sample. With the help of a polarizer in the detection optic, we found that the fifth harmonic was polarized parallel to the IR pulses, the spectral width of the observed signal being approx. $20\,\mathrm{cm^{-1}}$, i.e. typically twice

the width of the IR pulses. Changing the spectrometer center wavelength to 1 μm (in this spectral region, the sensitivity of the CCD array becomes rather low), we observed a third harmonic signal and, finally, around 480 nm (with a much longer integration time) a very weak seventh harmonic signal was detected.

Figure 2 shows the intensity dependence of the third and fifth harmonic intensity in a double logarithmic plot. The slopes of 3.01 ± 0.08 and 4.78 ± 0.13 are very close to the expected values for a third and fifth-order process. (The seventh-harmonic signal was too weak to be analyzed in detail.)

The frequency dependence of the integrated fifth-harmonic intensity (normalized with the fifth power of the input intensity) is shown in Fig. 3 (semilogarithmic plot). The signal is rather strong on the low-frequency side of the CH absorption of the chloroform molecules (maximun around $2850\,\mathrm{cm}^{-1}$ with a factor-of-ten decay within $150\,\mathrm{cm}^{-1}$ on both sides). Across the resonance frequency ($3020\,\mathrm{cm}^{-1}$; CH-stretching absorption of $CHCl_3$), the harmonic intensity goes down by a factor of more than 100 and then rises again by an order of magnitude.

The frequency dependence of the third harmonic was also registered; it is strongly influenced by the strongly decreasing spectral sensitivity of the CCD array on the long-wavelength side. Nevertheless, the results clearly show that the efficiency for pumping frequencies below $3000\,\mathrm{cm}^{-1}$ is much higher compared with the other side. The same statement is true for the observed seventh harmonic.

Finally, an estimate of the energy conversion efficiency for the harmonic generation can be given for the third, fifth, and seventh harmonic, estimates of approx. 3×10^{-8}, 10^{-10}, and 10^{-15} respectively are obtained.

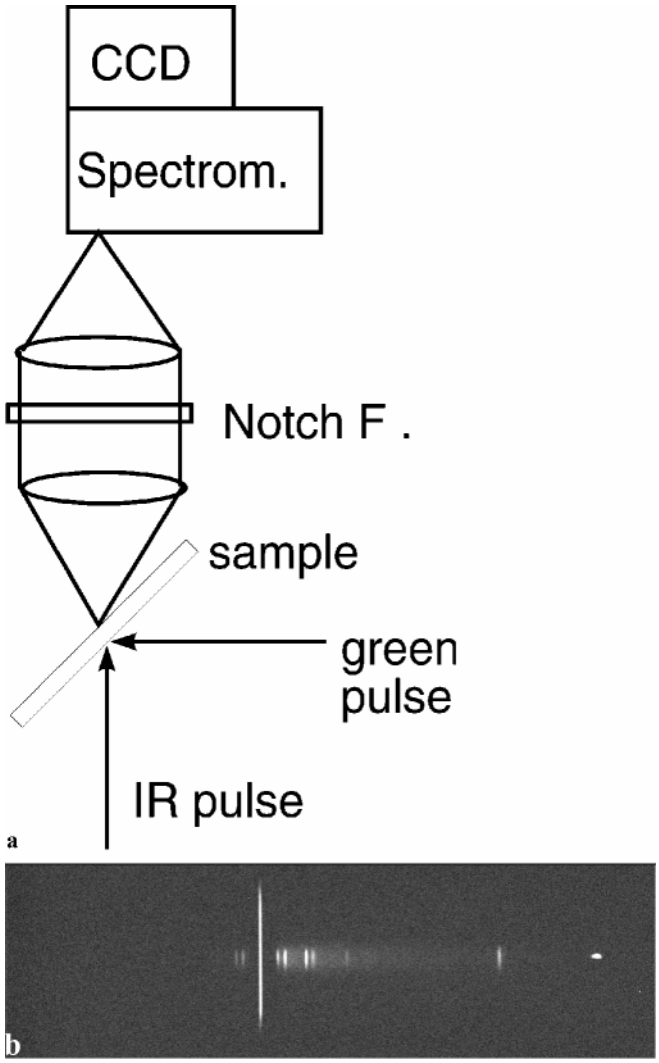

Fig. 1. a Scheme of the probe setup. **b** Image of the illuminated CCD camera. The strong vertical line is due to Rayleigh scattering, whereas the smaller ones originate in Raman scattering. An additional intensity with a different spatial shape can be seen at the right side of the picture

2 Interpretation and discussion

The discussion starts with the definitions of the pump field $E = 1/2 E_0 \exp(\mathrm{i}(\omega t - kz)) + \text{c.c.}$ and the field of the jth harmonic $E_j = 1/2 E_{j0} \exp(\mathrm{i}(\omega_j t - k_j z)) + \text{c.c.}$, both propagating in the z direction. The nonlinear polarization responsible for the generation of the jth harmonic is:

$$P_{\mathrm{NL}}^{(j)} \propto \chi^{(j)} (E_0)^j \exp(\mathrm{i}\Delta kz)\,, \tag{1}$$

where $\chi^{(j)}$ is the nonlinear susceptibility of jth order and

$$\Delta k = k_j - jk = \frac{j\omega}{c}(n_j - n) \tag{2}$$

is the phase mismatch, with c the velocity of light and n and n_j the refractive indices at the fundamental and harmonic frequencies, respectively. In (1) all indices indicating the polarization directions are omitted as all fields are polarized parallel.

For the description of evolution of the fields in the experimental situation (low conversion, no absorption of the generated harmonic), two differential equations can be derived following the standard procedure as given in the textbooks of nonlinear optics:

$$\frac{\mathrm{d}E_0}{\mathrm{d}z} = -\frac{\alpha}{2} E_0\,, \text{ and} \tag{3}$$

$$\frac{\mathrm{d}E_{j0}}{\mathrm{d}z} = \kappa j\omega \chi^{(j)} (E_0)^j \exp(\mathrm{i}\Delta kz)\,, \tag{4}$$

where κ is a constant and α the absorption coefficient for the fundamental. The solution of (3) is a simple exponential decrease $E_0(z) = E_0 \exp(-\alpha z/2)$. Inserting this in (4), integrating over z, and multiplying with the conjugate complex, we obtain for the generated harmonic intensity after a sample length L (no harmonic input):

$$I^{(j)} = \kappa' \left(\chi^{(j)}\right)^2 (j\omega)^2 (I_0)^j \eta\,, \text{ with}$$

$$\eta = \frac{1}{(j\alpha/2)^2 + \Delta k^2} \left(1 - 2\mathrm{e}^{(-(j\alpha/2)L)} \cos(\Delta kL) + \mathrm{e}^{(-j\alpha L)}\right), \tag{5}$$

representing an efficiency factor that includes the fundamental absorption losses by α and the phase mismatch

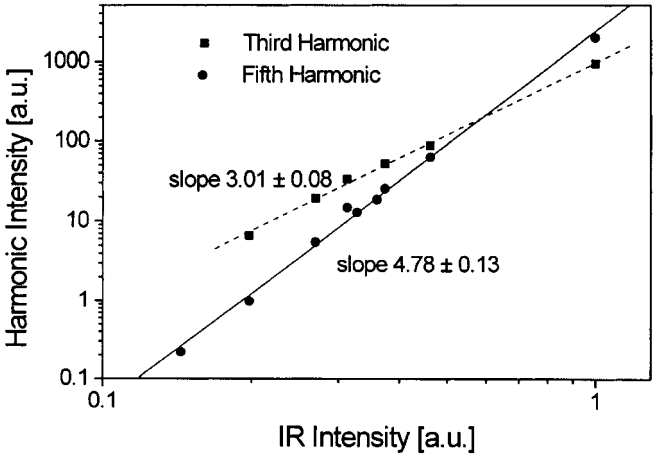

Fig. 2. Intensity dependence of the integrated third and fifth harmonic intensity (double log plot); infrared frequency 3000 cm^{-1}. The slopes of least mean square fits give 3.01 ± 0.08 (dashed line) and 4.78 ± 0.13 (solid line) respectively

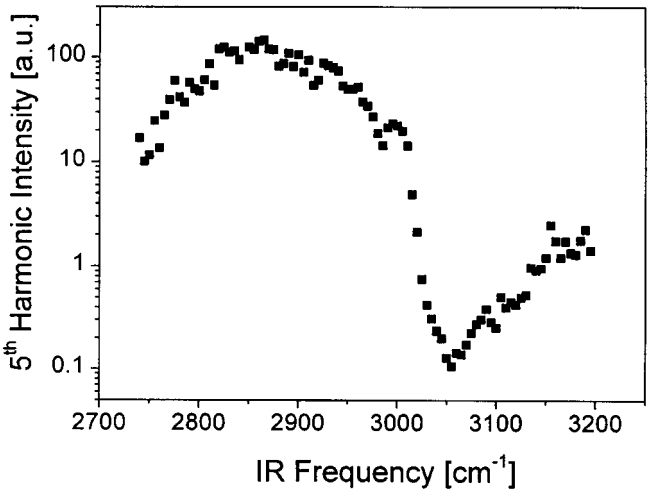

Fig. 3. Measured frequency dependence of the integrated fifth harmonic signal. The signal is normalized with the fifth power of the IR intensity

by Δk. Without absorption, η reduces to the well known $\sin^2(\Delta kL/2)/(\Delta k/2)^2$.

To evaluate the frequency dependence of the harmonic intensity, we need to model the $\chi^{(j)}$. Generalizing the corresponding expression for the resonantly enhanced third-harmonic generation [12, 13] (with one dominant resonance contribution) by introducing $j+1$ energy levels named $0, 1, \ldots j$, we obtain:

$$\chi^{(j)} \propto N \frac{\mu_{0,j} \prod_{m=1}^{j} \mu_{m,m-1}}{\prod_{m=1}^{j} \left(\mu_{m,0} - m\omega - \mathrm{i}\Gamma_{m,0}\right)}, \tag{6}$$

where $\omega_{i,j}$ is the energy difference between the levels i and j, $\Gamma_{i,j}$ is the width of the corresponding transition and $\mu_{i,j}$ is the transition dipole matrix element.

More detailed analysis requires assumptions about the introduced energy levels. As the pump pulse is close to a vibrational resonance (the CH-stretching vibration of chloroform), it is assumed that the harmonic generation is resonantly enhanced by this vibration. Starting with a harmonic oscillator model, we find that all factors in the denominator in (6) are minimal for the same frequency and the last j dipole matrix elements in the numerator are of the same order as for the fundamental transition, but the leading dipole matrix element is zero due to the strict selection rule for the harmonic oscillator $\Delta v = \pm 1$, allowing no harmonic generation at all. A cubic anharmonicity in the oscillator potential shifts the transition frequencies according $\omega_{j,0} = j\omega_0 - j(j+1)\Delta\omega$, where ω_0 is the harmonic frequency and $\Delta\omega$ the anharmonic shift. The perturbed wave functions ψ_j have contributions from $\psi^0_{j\pm1}$ and $\psi^0_{j\pm3}$ (where ψ^0_j are wave functions of the harmonic oscillator). In this approximation, nonvanishing dipole matrix elements $\mu_{0,j}$ (the leading factor in the fraction numerator in (6)) occur up to $j = 7$ and, correspondingly, reasonable contributions up to seventh-harmonic generation can be expected.

For chloroform, the anharmonic shift can be deduced from absorption spectra giving $\Delta\nu = 55\ cm^{-1}$. The linewidths $c\Gamma_{m0}/2\pi$ were estimated from absorption spectra (e.g. for the fundamental transitions 6 cm^{-1} were found). With these numbers, the frequency dependence of $\chi^{(j)}$ can be calculated. The generated harmonic is furthermore influenced by

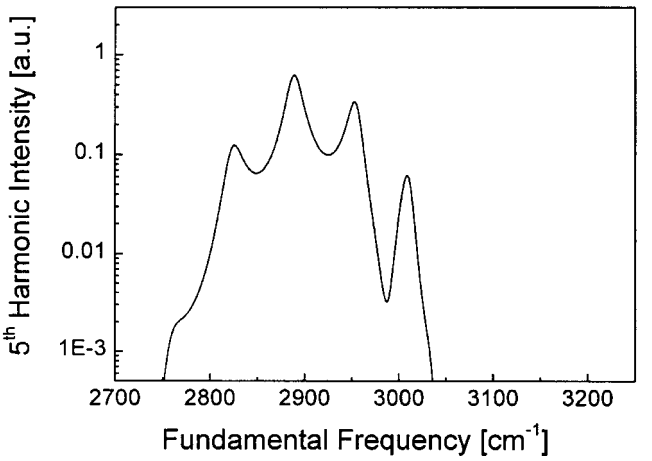

Fig. 4. Calculated frequency dependence of the fifth-harmonic intensity

the efficiency factor η (phase-matching, absorption losses; see (5)). This factor can be calculated using infrared absorption data [14] and visible refractive index data [15] (extrapolated by a Sellmeier type equation). The mismatch Δk (around 2900 cm^{-1}) is estimated to 650 cm^{-1}, giving an effective interaction length of approx. 100 μm. The calculated frequency dependence of the fifth-harmonic intensity is shown in Fig. 4. Due to well separated vibrational resonances in $\chi^{(5)}$, a clear structure is obtained. The sharp rise slightly below 3020 cm^{-1} is due to the fundamental absorption losses, which obviously reduce the harmonic generation; on the other hand, the refractive index variation around the absorption (Kramers–Kronig relation) results in a better phase matching on the low-frequency side.

The comparison between the experimental result (Fig. 3) and the calculated curve (Fig. 4) shows that the assumption of vibrationally enhanced harmonic generation seems to be correct; the frequency region of efficient generation is well reproduced by the calculation. The influence of the fundamental CH-stretching absorption at 3020 cm^{-1} (a sharp increase of the harmonic generation around this frequency) is well displayed. On the other hand, there are remarkable differences: first, except close to the resonance, (where the experimen-

tal data display a weak maximum), the calculated structure is hardly found in the experiment; and secondly, the calculation gives no high frequency component.

The above discussion is rather simplified. In the molecular model, only one fundamental vibrational state was introduced, whereas the real chloroform molecule has six fundamental vibrations each of which may contribute to the observed harmonic generation via anharmonic coupling, overtones and combination tones. By these additional contributions, the peaked structure of Fig. 4 may be smeared out. Furthermore, the calculation takes only one nonlinear process (harmonic generation via $\chi^{(5)}$) into account and neglects the effects of lower (and higher) order. For example, self-phase-modulation (a $\chi^{(3)}$ process neglected in (3)) will lead to a spectral broadening; correspondingly, the calculated spectral structure may be washed out.

In addition, the description for frequencies near the fundamental resonance is too simple. Under the experimental conditions discussed, a vibrational population of the CH-stretching mode of approx. 10% can be achieved (and was detected via spontaneous anti-Stokes Raman scattering). This will reduce the fundamental absorption losses (known as bleaching) and change the phase matching due to the corresponding refractive index changes [16]. Consequently, fifth-harmonic generation near the fundamental resonance, including vibrational excess population, must be described as an eight-wave mixing process by $\chi^{(7)}(-5\omega; \omega, -\omega, \omega, \omega, \omega, \omega)$.

The harmonic contributions on the high-frequency side (compare Figs. 3 and 4) can be explained as a contribution from the cell windows, where residual OH resonances may enhance this contribution.

An extrapolation of the efficiencies for shorter pulses and constant energy densities (as needed for population relaxation measurements) gives important results for those experiments. Using 200 fs IR pulses (compared with 4 ps used for the experiments described above), we would expect an efficiency increase by 3×10^6 for the fifth and 1.3×10^9 for the seventh harmonic; under those conditions, overall efficiencies up to 10^{-4} may be expected.

Finally, it will be interesting to perform similar experiments near vibrational resonance of lower frequencies, e.g. the CH-bending vibration of chloroform. If the above-given considerations are correct, we would expect a drastical increase of the efficiency: from the larger transition dipole moment and the smaller anharmonic shifts, which give a better overlap of the resonance factors in the denominator of (6), a larger $\chi^{(5)}$ is expected.

In addition, the lower dispersion in the IR will increase the interaction length, again giving a higher efficiency.

3 Conclusions

The generation of a fifth-harmonic signal of mid-IR pulses in simple liquids is reported. The analysis shows that the unexpectedly high conversion efficiency can be explained by a resonance enhancement within molecular vibrations. Further studies are needed to analyze and understand these processes in more detail; additionally it will be interesting to investigate the possibilities of high-harmonic generation in order to study details of molecular dynamics.

References

1. J. Reintjes, C.-Y. She, R.C. Eckardt: IEEE J. Quantum Electron. **QE-14**, 581 (1978)
2. M.D. Perry, G. Mourou: Science **264**, 917 (1994)
3. E.J. Heilweil, M.P. Cassassa, R.R. Cavanagh, J.C. Stephenson: J. Chem. Phys. **85**, 5003 (1986)
4. H. Graener, R. Dohlus, A. Laubereau: Chem. Phys. Lett. **140**, 306 (1987)
5. H. Graener, G. Seifert: J. Chem. Phys. **98**, 36 (1993)
6. G. Seifert, H. Graener: J. Phys. Chem. **98**, 11827 (1994)
7. H.J. Bakker, P.C.M. Planken, L. Kuipers, S. Lagendijk: J. Chem. Phys. **94**, 1730 (1991); H.J. Bakker, ibid. **98**, 8496 (1993)
8. A. Laubereau, D. von der Linde, W. Kaiser: Phys. Rev. Lett. **28**, 1162 (1972)
9. A. Tokmakoff, B. Sauter, A.S. Kwok, M.D. Fayer: Chem. Phys. Lett. **221**, 412 (1994)
10. M. Hofmann, H. Graener: Chem. Phys. **206**, 129 (1996)
11. M. Hofmann, R. Zürl, H. Graener: J. Chem. Phys. **105**, 6141 (1996)
12. A. Yariv: *Quantum Electronics* (Wiley, New York 1989)
13. J.J. Wynne, P.P Sorokin: In *Nonlinear Infrared Generation*, ed. by Y.-R. Shen (Springer, Berlin 1977) pp. 160–213
14. J.P. Hawranek, R.N. Jones: Spectrochim. Acta **32A**, 111 (1976)
15. Landolt-Börnstein: *Numerical data and functional relationships in science and technology: New Series III/38B* (Springer, Berlin 1992)
16. G. Seifert, H. Graener: Opt. Commun. **115**, 216 (1995)